

A new highly automated sputter equipment for in situ investigation of deposition processes with synchrotron radiation

Ralph Döhrmann, Stephan Botta, Adeline Buffet, Gonzalo Santoro, Kai Schlage et al.

Citation: *Rev. Sci. Instrum.* **84**, 043901 (2013); doi: 10.1063/1.4798544

View online: <http://dx.doi.org/10.1063/1.4798544>

View Table of Contents: <http://rsi.aip.org/resource/1/RSINAK/v84/i4>

Published by the [American Institute of Physics](http://www.aip.org).

Additional information on *Rev. Sci. Instrum.*

Journal Homepage: <http://rsi.aip.org>

Journal Information: http://rsi.aip.org/about/about_the_journal

Top downloads: http://rsi.aip.org/features/most_downloaded

Information for Authors: <http://rsi.aip.org/authors>

ADVERTISEMENT

physicstoday

Comment on any
Physics Today article.

Measured energy in Japan
David von Seggern
(dvseg@seismo.unr.edu) University of Nevada
July 2012, page 10
DIGITAL OBJECT IDENTIFIER
<http://dx.doi.org/10.1063/PT.3.1619>

Comment on this article
By the act of hitting a ball with a bat, one calculates the force energy to deliver the ball to its new location, but one must also take into account that the ball extended its energy to the entire team, which became struck by the ball as its momentum ceased and passed energy to the entire team. Therefore the parameters of the damage extend into the future when the received energy to that pushed upon, later becomes released in a new event. Perhaps calculations of one added that in, while another's calculations did not. E.M.C.
Written by Edgar Mocarvill, 14 July 2012 19:59

A new highly automated sputter equipment for *in situ* investigation of deposition processes with synchrotron radiation

Ralph Döhrmann,¹ Stephan Botta,¹ Adeline Buffet,¹ Gonzalo Santoro,¹ Kai Schlage,¹ Matthias Schwartzkopf,¹ Sebastian Bommel,^{1,2} Johannes F. H. Risch,¹ Roman Mannweiler,¹ Simon Brunner,³ Ezzeldin Metwalli,³ Peter Müller-Buschbaum,³ and Stephan V. Roth¹

¹DESY, Deutsches Elektronen-Synchrotron, Notkestrasse 85, D-22607 Hamburg, Germany

²Institut für Physik, Humboldt-Universität zu Berlin, Newtonstr. 15, D-12489 Berlin, Germany

³Lehrstuhl für Funktionelle Materialien, Physik-Department, Technische Universität München, James-Frank-Str. 1, D-85748 Garching, Germany

(Received 3 December 2012; accepted 12 March 2013; published online 3 April 2013)

HASE (Highly Automated Sputter Equipment) is a new mobile setup developed to investigate deposition processes with synchrotron radiation. HASE is based on an ultra-high vacuum sputter deposition chamber equipped with an in-vacuum sample pick-and-place robot. This enables a fast and reliable sample change without breaking the vacuum conditions and helps to save valuable measurement time, which is required for experiments at synchrotron sources like PETRA III at DESY. An advantageous arrangement of several sputter guns, mounted on a rotative flange, gives the possibility to sputter under different deposition angles or to sputter different materials on the same substrate. The chamber is also equipped with a modular sample stage, which allows for the integration of different sample environments, such as a sample heating and cooling device. The design of HASE is unique in the flexibility. The combination of several different sputtering methods like standard deposition, glancing angle deposition, and high pressure sputter deposition combined with heating and cooling possibilities of the sample, the large exit windows, and the degree of automation facilitate many different grazing incidence X-ray scattering experiments, such as grazing incidence small and wide angle X-ray scattering, in one setup. In this paper we describe in detail the design and the performance of the new equipment and present the installation of the HASE apparatus at the Micro and Nano focus X-ray Scattering beamline (MiNaXS) at PETRA III. Furthermore, we describe the measurement options and present some selected results. The HASE setup has been successfully commissioned and is now available for users. © 2013 American Institute of Physics. [<http://dx.doi.org/10.1063/1.4798544>]

I. INTRODUCTION

In process technology the deposition of thin films is often a crucial step for tailoring devices, micro- and nanostructures, and their final properties. During the different processing steps, several high-throughput techniques are used, ranging from liquid deposition, such as spray or dip coating,^{1,2} to vacuum deposition.^{3,4} For large scale and roll-to-roll applications the latter is especially useful and widely used. It allows bottom-up fabrication of designed compounds and morphologies with tailored catalytic, optical, or magnetic properties.^{5–13}

Radio Frequency (RF) sputter deposition is an industrial process extensively used to deposit thin films and, complementary to Direct Current (DC) sputter deposition, it allows to deposit both conducting and non-conducting materials.¹⁴ In order to better control and optimize the deposition process, it is essential to understand the kinetic phenomena involved in the thin film formation.¹⁵ For this kind of investigations, synchrotron radiation is a powerful tool enabling *in situ* and real-time experiments of kinetic processes.^{5,6,16–19} Moreover, grazing incidence X-ray scattering (GIXS) based techniques enable retrieving details of the nanostructure developed during the growth of thin films. The P03-beamline at PETRA III, also called Micro and Nano focus X-ray Scatter-

ing beamline (MiNaXS), has been optimized for performing small, ultra-small, and wide angle X-ray scattering in both transmission and grazing incidence geometries.^{20,21} Due to the excellent photon beam properties of the low emittance source PETRA III, the photon flux available at MiNaXS allows to perform brilliance demanding investigations such as *in situ* time-resolved experiments.^{20,21}

To use the full high-throughput capacity of the beamline for the study of kinetic processes, a highly automated sputter equipment (HASE) has been designed and built. Compared to commercially available sputter deposition devices, the HASE apparatus is extremely compact and flexible and must fulfill special requirements in order to be used at synchrotron beamlines. This apparatus can be integrated, for example, to the MiNaXS beamline, to carry out *in situ* investigations, with a temporal resolution on the order of milliseconds, on thin film formation during sputter deposition under variable experimental conditions.

The wide range of feasible deposition conditions such as deposition rate, orientation of deposition relative to the sample surface, co-sputter deposition, or to tune working gas pressure from low to high pressure (to tune kinetic energy of the sputter deposited atoms) enables to tune the material specific properties and those induced by the shape and crystallinity

of the deposited thin films and nanostructures. These experiments can provide very valuable information to better control and optimize the deposition process and thus, to better tailor the desired final properties of the deposited thin films. Anisotropic shapes of nanostructures and nanocrystals which are tilted with respect to the surface plane allow, for example, to tune the optical properties of asymmetrically shaped noble metals^{22–24} (surface plasmon resonance effect) or to induce a magneto crystalline anisotropy.

In this paper we describe in detail the requirements, operating options, and layout of the HASE deposition chamber, which is already in user operation, as well as the configuration of the HASE setup at the MiNaXS beamline. Selected results, illustrating the performance of the setup, are also presented.

II. TECHNICAL LAYOUT OF THE HASE APPARATUS

A. Design requirements

In order to perform *in situ* investigations during sputter deposition with the required flexibility, the apparatus not only has to fulfill the requirements of the sputter deposition process but also the additional demands for combining this process technology with the scattering geometries of GIXS, such as grazing incidence small and wide angle X-ray scattering (GISAXS and GIWAXS).

For the sputter processes an ultra-high vacuum (UHV) is essential to protect the deposited material from oxidation and contamination. Concurrently, the vacuum system should be able to handle high pressure sputtering conditions (larger than 10^{-1} mbar) which might be required during sputter deposition. Different sputter geometries such as glancing angle deposition (GLAD)^{25,26} and co-sputter experiments²⁷ should be feasible as well as heating and cooling of the sample substrate. Since the apparatus has been implemented in the P03 beamline to use GIXS methods, the sputter direction is downwards. A schematic drawing of the deposition chamber and of different sputtering processes in combination with GISAXS and GIWAXS is shown in Figure 1. Furthermore, the sputter chamber and the sample stage require precise and reproducible positioning. A safe and fast sample change, a modular concept with expandability and fully remote controlled operation is also required.

B. Mechanical design of the sputtering device

The apparatus is an independent and expandable equipment (Figure 2). On the one hand it can be used in the laboratory to deposit thin films and run tests. On the other hand it can be integrated at a beamline (particularly the MiNaXS beamline), to perform *in situ* investigations during sputter deposition. The modular construction of HASE facilitates installation at beamlines. The main components of the setup are described in this section.

1. Vacuum system

The HASE device consists of two independent vacuum chambers. The first chamber, which is actually the sputter de-

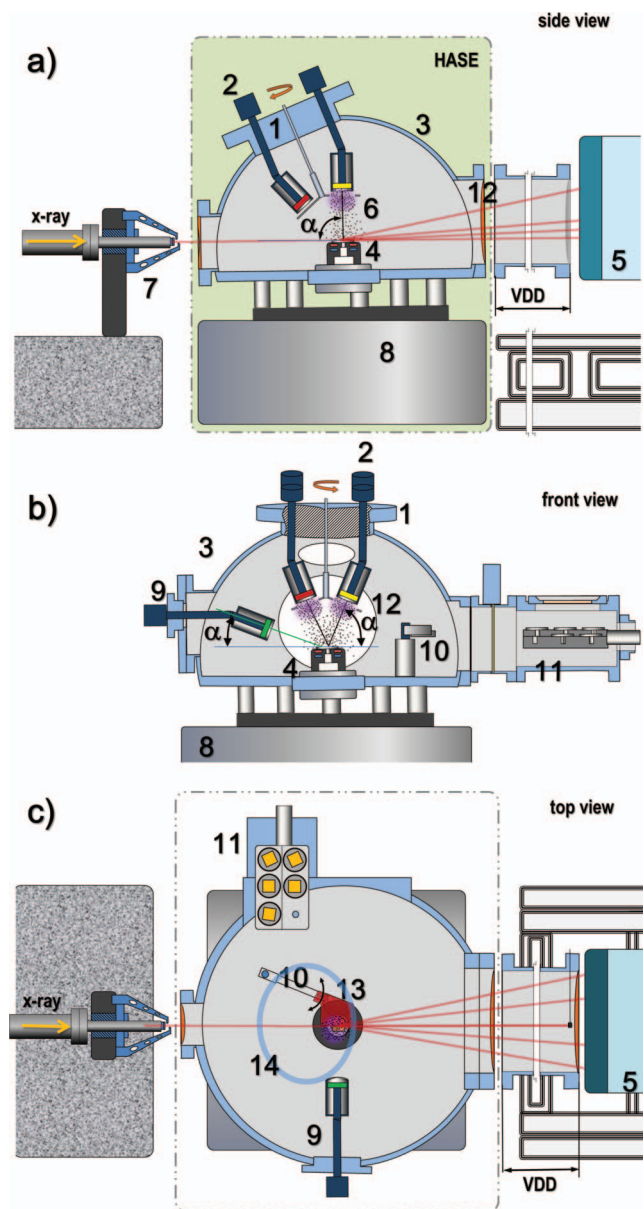


FIG. 1. Schematic drawing of the *in situ* GISAXS and GIWAXS measurements during different sputter deposition technologies with: (1) rotatable flange, (2) sputter guns, (3) vacuum deposition chamber, (4) sample stage, (5) X-ray detector, (6) plasma, (7) beam defining slit system, (8) sample positioning device, (9) additional sputter gun for GLAD sputter experiments, (10) sample change robot, (11) sample container, (12) exit window, (13) mask, and (14) position of the upper sputter flange. (a) Principle of standard sputter deposition. The components placed on the green background belong to the HASE-device. (VDD) variable distance to detector (0.1–10 m), (α) angle between sputter gun and sample surface the angle can be varied from 46° to 90°) by turning the upper rotatable flange (1). (b) Principle of co-sputter experiments. (c) Schematic sketch to show the possibility to install masks.

position chamber, includes the sputter guns, the sample stage, and the pick-and-place robot, to change the sample. The second chamber or transfer chamber is used for sample storage and includes an automatic sample transfer system (Figure 2). The sputter chamber is equipped with two turbo pumps (High-Pace300, Pfeiffer Vacuum, Germany) combined with a side channel backing pump (OnTool-Booster, Pfeiffer Vacuum, Germany). The use of these pumps, combined with a smart control of bypass and backing pump valves, enables both high

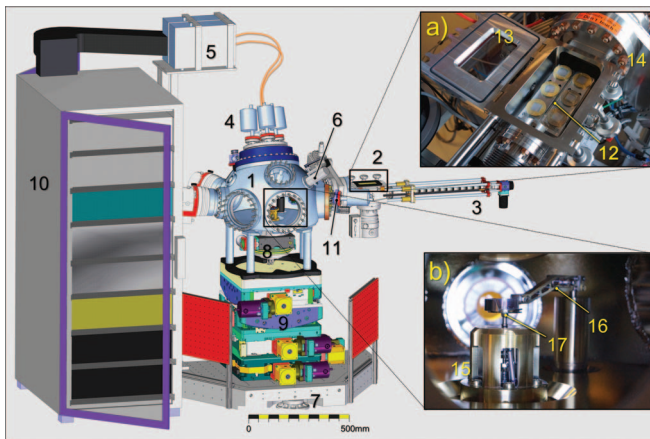


FIG. 2. Overview of the highly automated sputter equipment with (1) sputter deposition chamber, (2) transfer chamber with load lock, (3) sample transfer system, (4) sputter guns, (5) power supplies, (6) gas inlet valve, (7) air pads to move the system, (8) sample rotation stage, (9) sample positioning stage, (10) control-electronics rack, and (11) flange with an additional sputter gun. (a) Photograph of the transfer chamber with: (12) transfer arm, (13) load lock, and (14) transfer valve. (b) Photograph of the inner part of the chamber with: (15) sample stage, (16) pick-and-place robot, and (17) sample holder. The photograph shows the robot just before setting the sample holder into the sample stage.

pressure sputtering conditions, up to 5×10^{-1} mbar and high vacuum as low as 2×10^{-8} mbar base pressure. The transfer chamber is also equipped with a turbo pump (HighPace80, Pfeiffer), sharing the same backing pump. Venting and pumping of the transfer chamber to desired vacuum takes only a few minutes and does not influence the vacuum conditions in the sputter chamber.

2. Sputter deposition chamber

To enable precise positioning of the chamber relative to the beam, the construction does not exceed the maximum weight to be carried by the available multi axis positioning device^{20,21} used for alignment when performing *in situ* experiments. At the same time, the chamber is stable enough to enable automatic sample changing. The reliability of this automatic procedure requires very high form stability of the chamber and moving components. The stiff but light-weight design of both sputter and transfer chamber has been carried out using finite element method (FEM) calculations (ANSYS 12.1). The calculations confirmed that the form stability is sufficient. All critical deformations, which might complicate an automatic sample change, are below $40 \mu\text{m}$ and can be disregarded. The sample stage is located at the center of the chamber, thus the sample surface is in line with the entrance and exit windows and the intersection of the plasma cone provided by the sputter guns. The chamber also offers enough space to change the sample using a pick-and-place robot and for further modifications of the sample environment, e.g., application of external fields.

Up to four sputter guns are mounted on a rotatable flange attached to the chamber under a specific angle (Figure 1(a)). This construction enables to vary the glancing angle of sputter deposition in the range of $\alpha = 46^\circ\text{--}90^\circ$ with respect to the

sample surface. Besides, the arrangement of the sputter guns at this flange allows to exchange the working sputter gun during the operation of HASE, to enable a deposition of different materials on the same substrate, e.g., for the deposition of multi-layers. A remotely controlled shutter, which can be aligned in front of the sputter guns to prevent cross contamination, is also mounted on this flange.

3. Presently used windows

The chamber is equipped with an entrance-window for the synchrotron beam and two exit-windows for different scattering geometries shown in Figure 3. All window materials such as Beryllium, Kapton[®], Aluminum, and so on can be used depending on the wavelength of the synchrotron radiation and the scattered intensity of the deposited sample. The windows are necessary to ensure the desired flexible operation and the fast change from the laboratory to the beamline. For the experiments performed at P03 (13 keV) a Kapton window with a thickness of $25 \mu\text{m}$ has been used at the entrance side and a Kapton window with a thickness of $125 \mu\text{m}$ for the exit side. Both windows are covered with 100 nm aluminum to comply with the RF-safety regulations and to shield the sensitive detector electronic from the radio frequency field inside the chamber. The windows have been chosen in advance to ensure that they do not influence the collected scattering pattern. The exit windows with their large diameters of (x-win2) = 150 mm and (x-win3) = 100 mm enables the detection of scattering angles from $2\theta = 0^\circ\text{--}21^\circ$ and from 41° to 60° (Figure 3). In this configuration, a vacuum pressure of 2×10^{-7} mbar is accessible. For lower energies the setup is expandable to a full vacuum setup.

4. Transfer chamber

The transfer chamber is equipped with a load lock system (Figure 4), which comprises two sample carriers, a gate valve, a motorized sample transfer system, a quick-access door, and an observation window. Each sample carrier can be loaded with three sample holders (Figure 4(a)). The transfer system is able to lock in the carriers into the sputter chamber

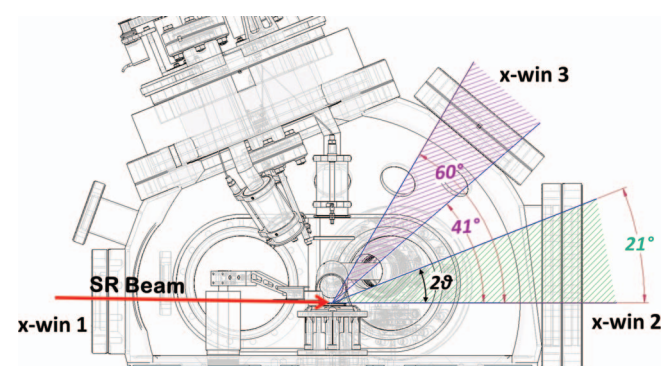


FIG. 3. X-ray scattering geometry characteristics of the HASE chamber. Beam entrance window is (x-win1). The GISAXS window (x-win2) enables the detection of scattering angles 2θ ranging from 0° to 21° . The upper window (x-win3) enables the detection of scattering angles 2θ ranging from 41° to 60° and can be used for GIWAXS and fluorescence measurements.

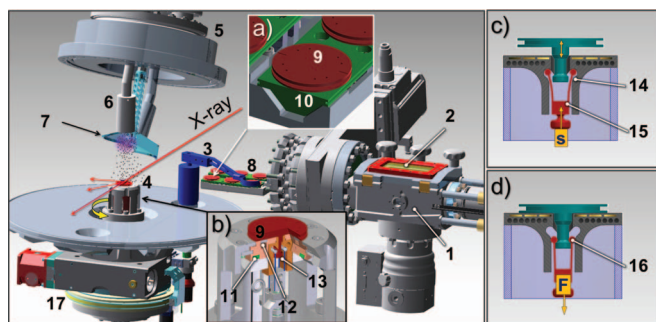


FIG. 4. View of the inner parts of the sputter chamber, of the transfer system and of the installed sample change robot with: (1) transfer chamber, (2) load lock, (3) pick-and-place robot, (4) sample stage, (5) rotatable flange, (6) sputter guns, (7) automated shutter, (8) transfer arm, and (17) goniometer for sample rotation. (a) Enlarged view of the sample transfer arm with: (9) sample holder and (10) sample carrier. (b) Enlarged view of the sample stage and the patented clamping device with: (9) sample holder, (11) ceramic heating element, (12) cooling channel, and (13) clamping device. The sample stage is mounted on a rotation feed through which enables a free rotation of $\pm 180^\circ$. (c) Schematic drawing of a released sample holder with: (14) curved track, (15) clamping claw, and (s) unclamp direction. (d) Schematic drawing of a fixed sample holder with: (16) fixture cylinders and (F) tension force direction.

without breaking the vacuum. Furthermore, it is possible to vent and evacuate the transfer chamber in a few minutes and the gate valve ensures that the vacuum conditions in the sputter chamber are not influenced by these processes.

5. Sample stage

The sample stage places the sample holder in a very accurate position in the center of the deposition chamber (Figure 4(b)) and is equipped with a heating/cooling device. Thus it is possible to vary the substrate temperature during sputter deposition, or in between the deposition of different coatings for annealing. The sample stage is equipped with ceramic heating elements allowing a maximum operation temperature of 200°C . A minimum temperature of -20°C can be reached by using cold nitrogen gas circulating through cooling channels. The sample holder is fixed with a patented clamping device,²⁸ which holds the sample holder with a defined force of 5 N ensuring an optimum contact between the sample holder and the tempered elements of the heating/cooling device. A schematic drawing of the heating and cooling device and the working mechanism of the clamping device is shown in (Figures 4(c) and 4(d)). The clamping from the lower side of the sample holder allows for a hemispherical space above the sample and arising thereby a 360° free field of view to the sample surface. The whole sample stage is mounted on a rotation feed-through, which is driven by a 1-circle goniometer (HUBER 411). This allows for a rotation of $\pm 180^\circ$ with an accuracy of 0.001° and for adjustment of the sample orientation, relative to the incoming X-ray beam. This is especially useful for GLAD deposition experiments.

6. Pick-and-place robot for sample changing

Quick and reliable change of the sample is a crucial issue to be considered in order to minimize idle time between sam-

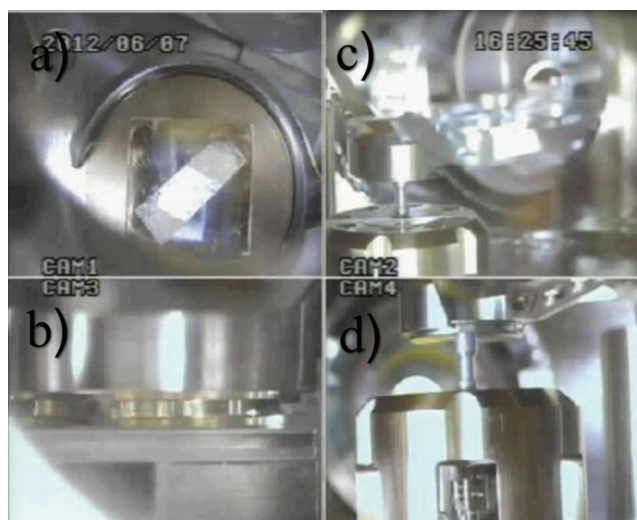


FIG. 5. Visualization of the sample transfer from four different points of view. (a) Top view of the transfer arm, (b) side view of the transfer arm, (c) view of the pick-and-place robot, and (d) view of the sample stage and clamping device (enhanced online) [URL: <http://dx.doi.org/10.1063/1.4798544.1>].

ples and, thus, optimize the use of the valuable beam at synchrotron radiation sources. For this purpose, the HASE system is equipped with a stepper motor driven sample change robot, which operates in the ultra-high vacuum (Figure 4). The sample change proceeds as follows: The robot arm lifts the sample holder containing the selected sample from the sample carrier and transfers it to the sample stage, inside the sputter chamber, where the sample holder is placed and clamped, see Figure 5. After finishing the sample change, the robot arm is moved to a ready-to-sputter position so as not to interfere with the sputter process or in the case of *in situ* experiments, shadow the scattered signal. The complete process involving the removal of a sample holder from the sample stage and the placing of a different sample holder takes less than 4 min.

7. Sputter sources

Up to four independent sputter sources can be installed at the upper rotatable flange. In this way, it is possible to perform deposition experiments or to deposit different materials on the same substrate (multilayer) without breaking the vacuum. As aforementioned, the rotatable flange is mounted under an angle of 22° to the sample surface. This advantageous arrangement of the sputter guns enables an automated adjustment of the sputtering angle in the range from $\alpha = 46^\circ$ – 90° to the sample surface (Figure 1(a)) making GLAD and co-sputtering experiments feasible.

At the time of this paper two sputter deposition guns are already available which can be used in parallel in combination with a remotely controlled shutter, to protect the sputter gun which is not in operation. The sputter guns were built by PLASSYS-Bestek SAS, France. The associated electronics was also delivered by PLASSYS. The electronic system configuration consists of a Controller (MC2), an matching network (AT-Series), and a RF power source generator (R301) (all components made by Seren IPS, USA.)

The Programmable Logic Controller (PLC) of the HASE apparatus interfaces to the MC2 matching network controller and the RF generator using TTL signals for start, stop, and veto signals, as well as analogue signals for controlling the output power. The maximum output power is 300 W at a frequency of 13.56 MHz. Each sputter gun is independent and can be controlled individually.

C. Electrical design

The control and power electronic components are assembled in a 19 in. electronic rack and can be moved together with the setup. This simplifies transport and setting up at the beamline. The whole apparatus is controlled by a PLC, which manages all functions and all input and output channels. The control system is equipped with an internal EtherCat bus and different terminals to link the connections to the electrical components of the setup. At the present operating status the PLC handles 24 digital inputs, 12 digital outputs, 8 analogue inputs, 8 analogue outputs, 8 relays outputs (potential free), and 6 stepper motor channels. This configuration ensures a beamline independent operation and allows for custom specific software sequences, e.g., defined sputter deposition programs. Furthermore, it allows for upgrading the equipment and a fail safe system.

The heating-cooling control system of the sample setup is based on a cryogenic temperature controller (LakeShore Model 340), which is available at the P03 beamline and can be operated independently in the laboratory or at the beamline.

D. Control software

HASE is controlled by a self-developed PLC control program based on TwinCat[®]. It manages all logical interconnections, safety conditions of the vacuum system, the computer numerical control of the stepper motors, and the sample change procedure. Furthermore, the program gates the output power of the sputter sources and triggers the sputtering time.

A Graphical User Interface (GUI) has access via handshake to all functions of the PLC and handles all operating controls of the HASE system. The HASE software is dedicated to control all functions of the equipment self-contained, but enables an easy integration into the beamline control software. This feature is essential for a remotely controlled operation of HASE and for a synchronized operation of sputter experiment and beamline equipment.

III. CONSIDERATIONS FOR SPUTTER DEPOSITION EXPERIMENTS

In order to perform several different sputter experiments with one setup at a synchrotron beamline, the apparatus has to be as flexible as possible. The following listed sputter deposition experiments and the combination of the different techniques can alternately be realized *in situ* with the HASE setup. In addition to these techniques, the sample environment with the heating/cooling device and the defined sample clamping

allows for further experiments with all the described deposition methods and technologies.

- *Standard sputter deposition:*
The principle is shown in Figure 1(a). “Standard sputter deposition” is the mostly used configuration. Here the Sputter deposition is performed at an angle of $\alpha = 90^\circ$ (to the sample surface).
- *Glancing angle deposition (GLAD):*
The principle is shown in Figure 1(a). In the GLAD configuration the deposition angle α can vary between 46° and 90° . If needed, an additional sputter gun can be mounted to reach a deposition angle of about 10° , as shown in Figure 1(b). The GLAD technique allows for the engineering of thin films composed of three-dimensional highly anisotropic nanostructures, which can be of great interest in electrical, optical,^{22–25,29} and magnetic applications.³⁰
- *Co-Sputter deposition:*
Two or more guns can be used to perform co-sputter deposition. In this case, different materials are sputtered simultaneously using the cluster of guns mounted on the rotatable flange (see Figure 1(b)). Here one can, for example, perform measurements during the self-organization or alloying of the deposited composite material.
- *Production of multi-layers:*
This method is depicted in Figure 1(a). In this case, layers of different materials are deposited successively. Prior to each layer deposition, the active gun is brought to the desired deposition position by an automated turning of the rotatable flange.
- *High pressure sputter deposition:*
Increase of the working gas pressure in the chamber (from 1×10^{-4} mbar to 5×10^{-1} mbar) is done up to the point that collision effects produce thermally cold atoms, which agglomerates in the gas phase.³¹ This allows for depositing clusters.³²
- *Mask-assisted sputter deposition:*
By using shadow masks one can influence the patterning of the thin films during deposition.³³ The masks can be placed in front of the substrate by using the sample robot arm. By moving the mask with the robot arm during the deposition it is, for example, possible to produce wedge gradient layers. The principle how to fix the mask is shown in Figure 1(c).

IV. CONSIDERATIONS FOR *IN SITU* SCATTERING EXPERIMENTS

The intensive and high brilliant beam available at P03 allows for a large number of different experiments with the described sputtering methods. The time resolution achieved, strongly depends on the photon flux available and on the detector used.

- *GISAXS and GIWAXS experiments:*
The large exit windows (shown in Figure 3) allow for a wide range of small and wide angle X-ray scattering experiments which can be measured simultaneously.

All sputtering experiments described above are feasible with the HASE apparatus. An *in situ* change between different sputter methods is practically possible.

- *Stop sputter experiments:*
Stop sputter experiment^{11,19,20} can also be performed to observe a layer-by-layer deposition. In this case a shutter is moved in front of the sputter gun to protect the sample from the source. To continue the deposition after depositing a certain amount of material the shutter can be swiveled out.
- *Magnetic fields at the sample:*
The robot arm used to change the sample can also be used to bring magnets close to the sample. In this way, one can apply variable magnetic fields to the sample after sputter deposition.

To complete the accuracy and the validity of the measurement results, additional measurement methods like reflectivity measurements can be performed after the sputter deposition.

V. INSTALLATION OF THE HASE SETUP AT THE MINAXS BEAMLINE

The HASE setup has mainly been specially designed and constructed to be installed at the Micro- and Nano focus X-ray Scattering beamline P03 at the PETRA III synchrotron storage ring, although it can in principle be mounted on other beamlines as well, if appropriate free space is provided. MiNaXS is dedicated to small and wide angle scattering experiments, using a micro- and nano-focused beam, in combination with low divergence and high flux.^{20,34}

The setup can be installed at the dedicated position for heavy weight sample environment at the beamline which is shown in Figure 6. The sputter device can be moved on air pads for coarse adjustment to the beam position. For the GISAXS and GIWAXS measurements the surface of the sample substrate needs a precise alignment to the beam. The sample position is fixed very accurately in the center of the sput-

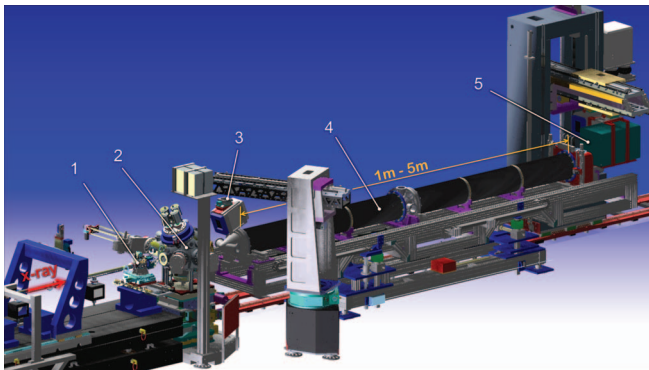


FIG. 6. HASE-apparatus setup in simultaneous GISAXS and GIWAXS geometry incorporated in the MiNaXS beamline. The illustration shows the possibility to install bulky equipment at an extended sample position behind the guard slits. (1) Optical bench with guard slit system, (2) sputter deposition chamber, (3) WAXS detector device with Pilatus 300K (Dectris, Switzerland), (4) variable flight tube, and (5) SAXS detector device with installed Pilatus 1M detector (Dectris, Switzerland).

ter deposition chamber. This fixation allows for a sample rotation in the range of $\pm 180^\circ$, by using a 1-circle goniometer (HUBER 411) which shows the yellow arrow in Figure 4. All other movements of the sample relative to the beam will be performed by using a multi-stage-goniometer (HUBER).²⁰ With this device it is possible to adjust the incidence angle, the height, the lateral position, and the lateral rocking angle of the sample with an accuracy of $\pm 1 \mu\text{m}$. The positioning device is able to carry a weight of 180 kg.

An adaptable evacuated flight tube with a tuneable length ranging from 1 m to 5 m is installed between the chamber and the X-ray detector.^{20,35} The flight tube can be tilted to cover also the angular regions needed for reflectivity measurements. Additional tube elements can be used to extend the distance between sample and detector to a maximum length of 10 m. This enables the performance of (grazing incidence) ultra-small angle X-ray scattering experiments (GI)USAXS.³⁶ During the measurements all functions of the HASE apparatus are controlled with signals from the beamline software and via Ethernet.

VI. SELECTED RESULTS

The functional capability of the sputter equipment has already been tested. In order to characterize the dependence of sputter rate on sputter power, *ex situ* X-ray reflectivity (XRR) measurements were performed at beamline E2 (DORIS III, DESY) to measure the effective film thickness after 300 s deposition of Au and Al on SiO_x substrates. The results, summarized in Table I, show a linear behaviour of the sputter rate versus the sputter power, as it has been already described for RF-sputter processes in the manufacturer's manual of the sputter sources.

To demonstrate the *in situ* capabilities of HASE at P03, we present two different results. The substrates for both cases were base-cleaned Si wafers and the sputtered material was Au. In both cases, Ar plasma was used for the deposition process.

Figure 7(a) depicts the GISAXS pattern after deposition of about 13 nm of Au on pre-cleaned Si. In this case, the sputter conditions were $P = 50 \text{ W}$ and $p(\text{Ar}) = 2 \times 10^{-2} \text{ mbar}$. Maxima in the 2D (GI)SAXS pattern, stemming from the Au nano-clusters formed on the surface are clearly observed. The data were acquired using a two-dimensional pixel detector (Pilatus 300K, Dectris, Switzerland) with a pixel size of $172 \times 172 \mu\text{m}^2$. The sample-to-detector distance was set to 4826 mm and a wavelength of $(0.0960 \pm 0.0002) \text{ nm}$ was

TABLE I. Sputter rates for Au and Al targets at different sputter powers at a sputter pressure of $1.5 \times 10^{-2} \text{ mbar}$.

Sputter power (W)	Sputter rate (nm/min)	
	Au	Al
50	0.8 ± 0.04	0.16 ± 0.01
100	1.44 ± 0.09	0.30 ± 0.07
150	...	0.43 ± 0.02
200	2.63 ± 0.08	...

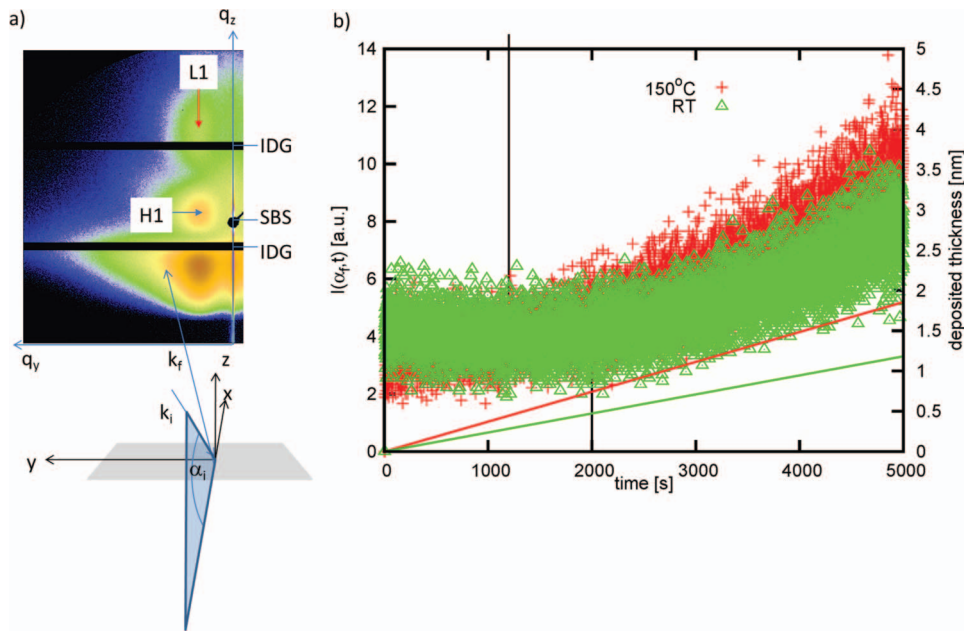


FIG. 7. (a) GISAXS (sample to detector distance = 4826 mm) of Au on SiO_x . To sketch the scattering geometry, we included a real space coordinate system $x/y/z$ and a reciprocal space coordinate system q_y and q_z . They are the wavevector transfers parallel and perpendicular to the sample surface. k_i and k_f denote the incoming beam and a scattered beam with $|k_i| = |k_f| = \frac{2\pi}{\lambda}$. α_i denotes the angle of the incoming beam to the sample surface (grazing angle). L1 denotes the side maxima produced by the presence of Au nanoclusters. H1 denotes the maxima in q_z -direction, stemming from the height of the nanoclusters. IDG denotes the intermodule gap of the detector and SBS denotes the point-like specular beam stop used to protect the detector from the high-intense specular reflection. (b) Scattered intensity versus time during sputter deposition of Au on SiO_x at two different substrate temperatures (green triangles 26 °C, red crosses 150 °C) in GIUSAXS geometry (sample-to-detector-distance 8650 mm). The intensity was extracted from a series of two-dimensional detector images at the reciprocal space point of $q_y = 0$, $q_z = 0.846 \text{ nm}^{-1}$. The two lines indicate a linear growth of the deposited thickness for both temperatures.

used. The incidence angle was $\alpha_i = 0.45^\circ$. q_y and q_z denote a reciprocal space coordinate system. They are the wavevector transfers parallel and perpendicular to the sample surface.

For *in situ* sputter deposition as a function of substrate temperature, the analysis of *in situ* time-resolved GIUSAXS data is presented in Figure 7(b). The data were acquired using a two-dimensional pixel detector (Pilatus 1M, Dectris, Switzerland) with a pixel size of $172 \times 172 \mu\text{m}^2$, a sample-to-detector distance of 8650 mm and a wavelength of $(0.0957 \pm 0.0002) \text{ nm}$. The incidence angle was $\alpha_i = 0.4518^\circ$ and 2 frames/s were recorded. This setup represents the unique combination of (GI)USAXS¹³ and sputter deposition available at P03 and, thus, the ability to follow the early stages of cluster formation and possibly nucleation with high angular and time resolution³⁶ probing correlated roughness changes in the sub-monolayer regime. Depicted is the intensity of the scattering pattern at $\alpha_f = 0.2864^\circ$ for deposition of Au ($P = 10 \text{ W}$, $p(\text{Ar}) = 1.5 \times 10^{-2} \text{ mbar}$) at two different substrate temperatures: 26 °C and 150 °C. The sputter deposition time ranges from 0 to 5000 s. In both cases the sputter rate is equal. It is clearly observed that at 150 °C the intensity curve starts to increase earlier and with a steeper slope, indicating a faster nanostructural build-up of Au nanoclusters at this temperature. We note, that the scattered intensity in grazing incidence geometry is governed by refraction and reflection effects.⁶ Additionally, the diffusely scattered intensity depends strongly on the effective density ρ , the type of roughness, and cluster arrangement installed. Especially in the early stages of nucleation, no diffraction pattern is visible, only a change in roughness due to the deposited sub-monolayers.

We therefore chose to monitor the diffusely scattered intensity between the material sensitive Yoneda peak ($\alpha_c \propto \rho$) and the specular peak, which is shielded by a beam stop to avoid saturation of the detector. We compared the final-deposited thickness using XRR. Assuming a linear dependence of the deposited mass as a function of time, we added the sputter deposited thickness, being proportional to the number of deposited atoms, as a function of time. This clearly shows the difference in structural build-up depending on the temperature. A detailed analysis is underway and not in the scope of this paper.

VII. SUMMARY AND OUTLOOK

To summarize, the design of the sputter chamber has been proven to be very useful for *in situ* experiments relying on high-throughput and fast acquisition. The design of HASE is unique in the flexibility so that it is possible to combine different sputter deposition methods in one setup, or to change between the methods automatically. Producing of single-layer, multilayer, wedge-gradient layers adapted for micro-focussing is as well possible as performing GLAD sputter deposition under various angles. The empty space in the chamber and around the sample, and the large exit windows facilitate many different *in situ* GIXS experiments and allow in addition for simultaneous measurements of (GI)WAXS and (GI)SAXS/USAXS.

The sample change works smoothly and allows a remote controlled sample change in less than 4 min. This tremendously increases the number of experiments that can be

performed within one measuring period or beamtime. The sample heating stage is able to reach rate and hold the required temperatures with a heating rate of about 1.2 K s^{-1} and cooling of the sample is also possible.

The setup has been successfully integrated into the beamline P03 at the PETRA III storage ring and generates promising results. The performed experiments show the *in situ* measurement possibilities in GISAXS geometry as well as in GIUSAXS geometry at different substrate-temperatures and two of this have been presented here. These investigations allow for determining the temperature dependence of thin film growth kinetics and their influence on surface morphology. The large exit window allows in addition for *in situ* reflectivity measurements to obtain information on the layer thickness and roughness at the time of the experiment. The modular construction of the sample stage enables the integration of different sample environments, such as high temperature (up to 900°C) or magnetic field equipment. These sample environments are currently under development. The pick-and-place robot arm, which is installed in the chamber to change the sample, offers the possibility to mount additional equipment, i.e., the installation of magnets or masks. Furthermore, GLAD-sputter experiments under a sputter angle of $\alpha = 10^\circ$ (position 9 in Figure 1(b)) and the implementation of additional optical characterization methods are foreseen.

ACKNOWLEDGMENTS

We would like to thank Dimitri Novikov (DESY) and Carsten Richter (DESY, TU Freiberg) for their help concerning the reflectivity measurements and the fits of the XRR measurements, as well as Reinhard Eisenberg (DESY) for the preparation of the video film.

- ¹A. Buffet, M. Abul-Kashem, J. Perlich, G. Herzog, M. Schwartzkopf, R. Gehrke, and S. V. Roth, *Adv. Eng. Mater.* **12**, 1235 (2010).
- ²J. Perlich, M. Schwartzkopf, V. Körstgens, D. Erb, J. F. H. Risch, P. Müller-Buschbaum, R. Röhlberger, S. V. Roth, and R. Gehrke, *Phys. Status Solidi (RRL)* **6**, 253 (2012).
- ³J. G. Han, *J. Phys. D: Appl. Phys.* **42**, 043001 (2009).
- ⁴S. Schiller, K. Goedicke, V. Kirchhoff, and C. Metzner, *Vak. Forsch. Prax.* **7**(4), 286 (1995).
- ⁵B. Krause, S. Darma, M. Kaufholz, H.-H. Gräfe, S. Ulrich, M. Mantilla, R. Weigel, S. Rembold, and T. Baumbach, *J. Synchrotron Radiat.* **19**, 216 (2012).
- ⁶G. Renaud, R. Lazzari, C. Revenant, A. Barbier, M. Noblet, O. Ulrich, F. Leroy, J. Jupille, Y. Borensztein, C. Henry, J. P. Deville, F. Scheurer, J. Mane-Mane, and O. Fruchart, *Science* **300**, 1416 (2003).
- ⁷H. Walter, G. Bauer, R. Dornick, G. Jakopic, and A. Leitner, *Opt. Eng.* **45**, 103801 (2006).
- ⁸S. V. Roth, H. Walter, M. Burghammer, C. Riekel, B. Lengeler, C. Schroer, M. Kuhlmann, T. Walther, A. Sehrbrock, R. Dornick, and P. Müller-Buschbaum, *Appl. Phys. Lett.* **88**, 021910 (2006).

- ⁹S. V. Roth, M. Burghammer, C. Riekel, P. Müller-Buschbaum, A. Diethert, P. Panagiotou, and H. Walter, *Appl. Phys. Lett.* **82**, 1935 (2003).
- ¹⁰A. Buffet, M. Abul-Kashem, K. Schlage, S. Couet, R. Röhlberger, A. Rothkirch, G. Herzog, E. Metwalli, R. Meier, G. Kaune, M. Rawolle, P. Müller-Buschbaum, R. Gehrke, and S. V. Roth, *Langmuir* **27**, 343 (2011).
- ¹¹K. Schlage, S. Couet, S. V. Roth, U. Vainio, R. Rueffer, M. Abul-Kashem, P. Müller-Buschbaum, and R. Röhlberger, *New J. Phys.* **14**, 043007 (2012).
- ¹²K. Sarathlal, D. Kumar, V. Ganesan, and A. Gupta, *Appl. Surf. Sci.* **258**, 4116 (2012).
- ¹³S. V. Roth, R. Döhrmann, M. Dommach, M. Kuhlmann, I. Kroeger, R. Gehrke, H. Walter, C. Schroer, B. Lengeler, and P. Müller-Buschbaum, *Rev. Sci. Instrum.* **77**, 085106 (2006).
- ¹⁴H. Greve, A. Biswas, U. Schuermann, V. Zaporozhchenko, and F. Faupel, *Appl. Phys. Lett.* **88**, 123103 (2006).
- ¹⁵S. Schiller, U. Heisig, C. Kkorndorfer, G. Beister, J. Reschke, K. Steinfeld, and J. Struempfel, *Surf. Coat. Technol.* **33**, 405 (1987).
- ¹⁶S. Couet, Ph.D. dissertation, University of Hamburg, Germany, 2008.
- ¹⁷E. Metwalli, S. Couet, K. Schlage, R. Röhlberger, V. Körstgens, M. Ruderer, W. Wang, G. Kaune, S. V. Roth, and P. Müller-Buschbaum, *Langmuir* **24**, 4265 (2008).
- ¹⁸G. Kaune, M. Ruderer, E. Metwalli, W. Wang, S. Couet, K. Schlage, R. Röhlberger, S. V. Roth, and P. Müller-Buschbaum, *ACS Appl. Mater. Interfaces* **1**, 353 (2009).
- ¹⁹G. Kaune, E. Metwalli, R. Meier, V. Körstgens, K. Schlage, S. Couet, R. Röhlberger, S. V. Roth, and P. Müller-Buschbaum, *ACS Appl. Mater. Interfaces* **3**, 1055 (2011).
- ²⁰A. Buffet, A. Rothkirch, R. Döhrmann, V. Körstgens, M. Abul-Kashem, J. Perlich, G. Herzog, M. Schwartzkopf, R. Gehrke, P. Müller-Buschbaum, and S. V. Roth, *J. Synchrotron. Radiat.* **19**, 647 (2012).
- ²¹S. V. Roth, G. Herzog, V. Körstgens, A. Buffet, M. Schwartzkopf, J. Perlich, M. Abul-Kashem, R. Döhrmann, R. Gehrke, A. Rothkirch, K. Stasig, W. Wurth, G. Benecke, C. Li, P. Fratzl, M. Rawolle, and P. Müller-Buschbaum, *J. Phys. Condens. Matter* **23**, 254208 (2011).
- ²²K. Robbie, M. J. Brett, and A. Lakhtakia, *Nature (London)* **384**, 616 (1996).
- ²³M. M. Hawkeye and M. J. Brett, *J. Vac. Sci. Technol.* **25**, 1317 (2007).
- ²⁴M. Mansour, A. Keita, B. Gallas, J. Rivory, A. Besnard, and N. Martin, *Opt. Mater.* **32**, 1146 (2010).
- ²⁵K. Robbie, M. J. Brett, and A. Lakhtakia, *J. Vac. Sci. Technol.* **16**, 1115 (1998).
- ²⁶A. Dolatshahi-Pirouz, T. Jensen, T. Vorup-Jensen, R. Bech, J. Chevallier, F. Besenbacher, M. Foss, and D. Sutherland, *Adv. Eng. Mater.* **12**, 899 (2010).
- ²⁷F. Faupel, V. Zaporozhchenko, T. Strunskus, and M. Elbahri, *Adv. Eng. Mater.* **12**, 1177 (2010).
- ²⁸R. Döhrmann, DESY US Patent PTC/EP2010/006052 (submitted 2 October 2009).
- ²⁹L. Simonot, D. Babonneau, S. Camelio, D. Lantiat, P. Guerin, B. Lamongie, and V. Antad, *Thin Solid Films* **518**, 2637 (2010).
- ³⁰S. Camelio, D. Babonneau, D. Lantiat, L. Simonot, and F. Pailloux, *Phys. Rev. B* **80**, 155434 (2009).
- ³¹P. Taneja, R. Chandra, R. Banerjee, and P. Ayyub, *Scr. Mater.* **44**, 1915 (2001).
- ³²C. Xirouchaki and R. E. Palmer, *Philos. Trans. R. Soc. London, Ser. A* **362**, 117 (2004).
- ³³R. Kummamuru, L. Hu, L. Cook, M. Y. Efremov, E. A. Olson, and L. H. Allen, *J. Micromech. Microeng.* **18**, 095027 (2008).
- ³⁴C. Krywka, H. Neubaue, M. Priebe, T. Salditt, J. Keckes, A. Buffet, S. Roth, R. Döhrmann, and M. Müller, *J. Appl. Crystallogr.* **45**, 85 (2012).
- ³⁵R. Döhrmann, S. Gogolin, A. Buffet, and S. V. Roth, HASYLAB Annual Report 2011, p. 108.
- ³⁶P. Müller-Buschbaum, E. Bauer, E. Maurer, S. V. Roth, R. Gehrke, M. Burghammer, and C. Riekel, *J. Appl. Crystallogr.* **40** (Supplement), s341–s345 (2007).